Analysis of the 2021 Semangko Bay Earthquake Sequence in Southern Sumatra, Indonesia, Using Broadband Seismic Network Data

Pepen Supendi[*1,2], Sri Widiyantoro[3,4], Nicholas Rawlinson[1], Adhi Wibowo[2], Priyobudi Priyobudi[2], Kadek Hendrawan Palgunadi[5], Andri Dian Nugraha[3], Iswandi Imran[6,7], Gayatri Indah Marliyani[8], Daryono Daryono[2], Bambang Setiyo Prayitno[2], Muhammad Sadly[2], Dwikorita Karnawati[2], Novita Sari[2], and Anton Sugiharto[2]

Abstract

Beginning on 30 June 2021, hundreds of earthquakes were detected beneath Semangko Bay in southernmost Sumatra, which is located adjacent to the Sunda Strait, a narrow sea passage that separates the islands of Java and Sumatra. A number of these earthquakes were large enough to be felt by people living in the city of Lampung, some 100 km to the east. In terms of magnitude and temporal distribution, the earthquakes did not follow a typical mainshock–aftershock sequence because the onset was marked by a cluster of five earthquakes with local magnitudes that ranged between 4.2 and 4.6, followed by a rapid decay in the number of detected events. We have relocated 254 of the 258 earthquakes that were recorded between 30 June and 14 July 2021, with a local magnitude range between M_L 0.9 and 4.6, using the double-difference relocation method (hypoDD); focal mechanisms were also determined for a subset of events with a magnitude > 4. Our results show that the seismicity pattern and focal mechanism solutions are more consistent with a multiple event episode caused by the rupture of several antithetic faults that have a similar strike to the west Semangko fault in southernmost Sumatra rather than a single fault plane. These faults appear to be part of a small graben system located beneath Semangko Bay, which was likely activated by ongoing extension in the Sunda Strait.

Cite this article as Supendi, P., S. Widiyantoro, N. Rawlinson, A. Wibowo, P. Priyobudi, K. H. Palgunadi, A. D. Nugraha, I. Imran, G. I. Marliyani, D. Daryono, *et al.* (2022). Analysis of the 2021 Semangko Bay Earthquake Sequence in Southern Sumatra, Indonesia, Using Broadband Seismic Network Data, *Seismol. Res. Lett.* **XX**, 1–9, doi: 10.1785/0220210304.

Supplemental Material

Introduction

Southernmost Sumatra (Fig. 1) lies within a transitional zone that accommodates a change from oblique subduction of the oceanic Indo-Australian plate beneath Sumatra to nearly trench-perpendicular subduction beneath Java (Hamilton, 1979). Structural control of the Sumatra mainland is dominated by the great Sumatra fault, extending from the Andaman transform fault system in the north to the Sunda Strait in the south. The great Sumatra fault has been separated into 19 segments that exhibit differential motion (Sieh and Natawidjaja, 2000), although this was recently updated to 40 segments (Irsyam *et al.*, 2017). Based on paleomagnetic data, the opening of the Sunda Strait likely occurred during the Pliocene as a result of clockwise rotation of Sumatra with reference to Java (Ninkovich, 1976; Nishimura *et al.*, 1986; Mukti, 2018). This may have accelerated transtensional deformation of the Semangko graben in the western Sunda Strait and transpressional deformation of the Krakatau graben in the eastern Sunda Strait (Schlüter *et al.*, 2002). Apart from the rotation of Sumatra, the formation of Sunda Strait is also associated with clockwise motion of the Sumatra sliver plate (Huchon and Le Pichon, 1984), a forearc wedge separated by the subduction thrust, and a strike-slip fault that

1. Department of Earth Sciences—Bullard Labs, University of Cambridge, Cambridge, United Kingdom, https://orcid.org/0000-0002-9784-9865 (PS); https://orcid.org/0000-0002-6977-291X (NR); 2. Agency for Meteorology, Climatology, and Geophysics, Jakarta, Indonesia; 3. Global Geophysics Research Group, Faculty of Mining and Petroleum Engineering, Institut Teknologi Bandung, Bandung, Indonesia, https://orcid.org/0000-0002-8941-7173 (SW); https://orcid.org/0000-0002-4844-8723 (ADN); 4. Faculty of Engineering, Maranatha Christian University, Bandung, Indonesia; 5. Physical Science and Engineering, King Abdullah University of Science and Technology, Thuwal, Saudi Arabia, https://orcid.org/0000-0002-3550-7341 (KHP); 6. Structural Engineering Research Group, Faculty of Civil and Environmental Engineering, Institut Teknologi Bandung, Bandung, Indonesia; 7. Center for Research on Disaster Mitigation, Institut Teknologi Bandung, Bandung, Indonesia; 8. Geological Engineering Department, Gadjah Mada University, Yogyakarta, Indonesia, https://orcid.org/0000-0003-1356-9645 (GIM)

*Corresponding author: ps900@cam.ac.uk

accommodates trench-parallel slip in the overriding plate. Based on multichannel reflection seismic data, Schlüter *et al.* (2002) suggest that besides the Semangko graben, what they identify as the Krakatau graben is now covered by volcanic material. Graben formation in this area is closely related to the stepover zone between the great Sumatra fault and the Ujung Kulon fault (Susilohadi *et al.*, 2009).

Based on their relative timing and ranges of magnitudes, seismic sequences have been classified by Mogi (1963) into three types, that is, (1) foreshocks–mainshock–aftershocks; (2) mainshock–aftershocks; and (3) swarm. Swarm earthquakes are typically characterized by continuous seismic activity of relatively small magnitude without any major earthquakes. A mainshock is larger than any foreshock or aftershock, but there is no universally accepted definition of the minimum magnitude difference Δm. Based on earthquakes recorded in New Zealand, Evison and Rhoades (1993) define mainshocks (M_1) in a mainshock–aftershock sequence ($M_{1,2,\ldots,N}$, in which N is the number of events in the sequence) to lie in the range M_1–$M_3 \geq 0.9$ or M_1–$M_3 = 0.8$ and M_1–$M_4 \geq 1.0$, in which $M_{1-4} > 3.6$. Helmstetter and Sornette (2003) investigate the applicability of Båth's law, which states that the average difference in magnitude between a mainshock and its largest aftershock is 1.2 irrespective of the magnitude of the mainshock using the epidemic-type aftershock sequence model of seismicity. They find that it is a reasonable approximation in a limited range of circumstances but varies with aftershock productivity and mainshock magnitude. However, for a variety of realistic parameters, mainshocks of magnitude ~4.5 tend to have an average Δm in the vicinity of 1.

Recently, an earthquake sequence took place in Semangko Bay, southern Sumatra (Fig. 1), starting on 30 June 2021. As of 14 July 2021, the Indonesian Agency for Meteorology, Climatology, and Geophysics (Badan Meteorologi, Klimatologi, dan Geofisika [BMKG]) recorded 258 events of local magnitude (M_L) <5 and an average depth >10 km. Even though these earthquakes have not caused damage and economic loss, some were felt and registered as high as II–III on the modified Mercalli intensity scale.

In this study, we compute precise hypocenter locations and focal mechanisms of events in the recent Semangko Bay earthquake sequence with the aim of determining the position, geometry, slip, and origin of the underlying faults that have ruptured.

Data and Method

The arrival-time dataset used in this analysis spans 30 June to 14 July 2021 and was collected from permanent BMKG seismic network stations (Nanometrics Trillium 120Q seismometers with a flat response between 120 s and 150 Hz, coupled with Trident Digitisers with sampling rates of 20–50 Hz) in southern Sumatra and western Java (Fig. 1). The quality of the data at two typical sites is illustrated in Figure S2, available in the supplemental material to this article, in the form of probabilistic power spectral density plots, which demonstrate the high signal-to-noise ratio across much of the short- and long-period bands. As a result, 258 earthquakes with local magnitudes of M_L 0.9–4.6 (Fig. 2) were detected and located in Semangko Bay based on the extraction of 1,972 *P*-wave and 1,462 *S*-wave arrival times from data recorded by 23 seismic stations (see Fig. 1). Based on the magnitude and event distribution as a function of time (Fig. 2), the seismicity does not naturally conform to either a mainshock–aftershock sequence or swarm seismicity. On one hand, it exhibits the typical exponential decay in the number of events over time that is characteristic of an aftershock sequence, yet it does not have an obvious mainshock. Although the largest earthquake (M_L 4.6) occurs near the start of the sequence, it is accompanied by four earthquakes (one before and three after) of $M_L > 4.2$. This is more in keeping with a "multiple event" sequence, as described by Console *et al.* (2020), for which the onset of seismicity is marked by several events that are of similar magnitude, followed by a more typical aftershock sequence. Such sequences have been observed in central Italy, and although the underlying physics is not well understood, it is thought that pore-pressure diffusion of underground fluids may be a factor. Our use of "multiple event" sequence is also consistent with the study of Evison and Rhoades (1993), who define multiple event sequences in New Zealand using the criteria $M_{1-4} \geq 3.3$, M_1–$M_3 \leq 0.7$, or M_1–$M_3 = 0.8$, and M_1–$M_4 \leq 0.9$, in which the subscript refers to the temporal order of the earthquakes.

For the earthquake location task, BMKG used the LocSAT linear inversion scheme (Bratt and Nagy, 1991), which is embedded in the SeisComP3 program (Hanka *et al.*, 2010) and exploits the IASP91 reference velocity model (Kennett and Engdahl, 1991). We then applied VELEST (Kissling *et al.*, 1994) to obtain a 1D velocity profile via a joint velocity-hypocenter inversion that used CRUST 1.0 (Laske *et al.*, 2013) (see Fig. S1) as a starting model.

Following the application of VELEST, the double-difference relocation method (hypoDD) program (Waldhauser, 2001) is applied to relocate hypocenters using a double-difference method (Waldhauser and Ellsworth, 2000). Underlying this method is an assumption that the distance between earthquake pairs is small compared with the distance to the respective station that recorded them, thus permitting an approximation that the corresponding ray paths essentially follow the same trajectory. For each event, *P* and *S* arrival-time catalog data were searched to identify paired events with similar travel times. The hypocentral separation maximum was set to 50 km, the maximum number of neighbors per event was set to 50, and the minimum number of links needed to define neighbors was set to 8. We imposed a maximum distance between cluster centroid and station of 150 km. These input parameter choices were made after extensive testing to determine the combination of values that achieved the best results,

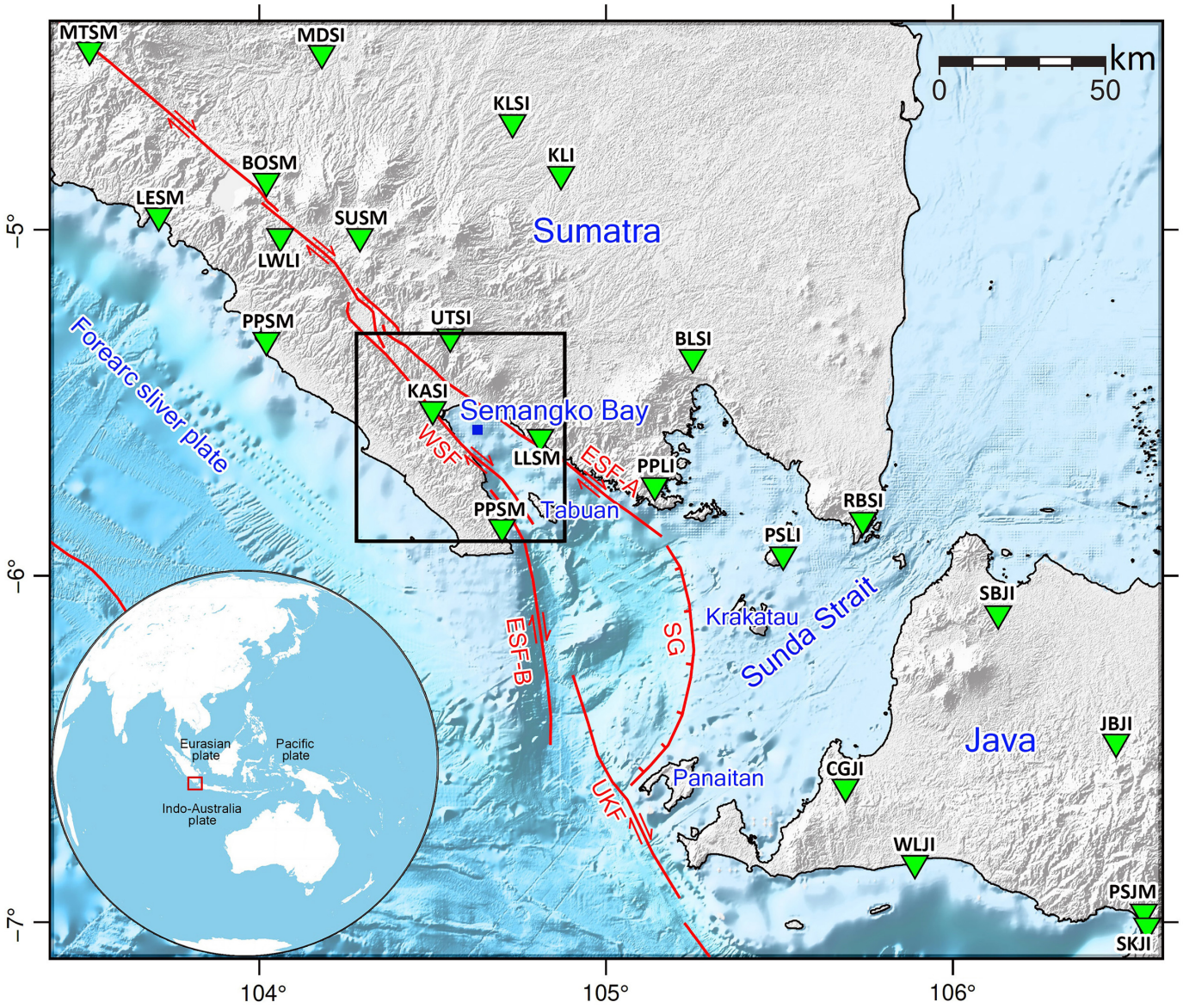

Figure 1. Map of the study area (within the black box). The green inverted triangles are Badan Meteorologi, Klimatologi, dan Geofisika (BMKG) stations in southern Sumatra and western Java. The red traces denote major crustal faults in the region sourced from Irsyam *et al.* (2017). Fault name abbreviations: ESF-A, east Semangko fault-A; ESF-B, east Semangko fault-B; SG, Semangko graben; UKF, Ujung Kulon fault; WSF, west Semangko fault. The regional location of the study area is indicated in the inset. The color version of this figure is available only in the electronic edition.

noting that the final distribution of relocated hypocenters does not change significantly across a reasonable range of input values.

Similar to the article by Supendi *et al.* (2021), we assess location uncertainty through application of a statistical resampling scheme based on the "bootstrap" method (Efron, 1982; Billings, 1994; Shearer, 1997). Using the final hypocenters (Fig. 3), samples were randomly drawn (with replacement) from the full set of observed residuals and used as replacements for each measurement; events were then relocated with the resampled dataset and the resultant shifts in location analyzed. As part of this test, we also added Gaussian noise with a standard deviation 0.1 s to the data to simulate the effect of picking error. The process was then repeated 200 times. The cumulative result is summarized in Figure 4 where error ellipses are plotted that contain 95% of the 200 points (for each event) obtained from the bootstrap locations.

For selected events ($M_L > 4$), we utilized the ISOLated Asperities package (Sokos and Zahradnik, 2008) to invert waveform data from the BMKG stations (see inverted green triangles in Fig. 1) to retrieve moment tensor solutions. This package combines least squares minimization to constrain moment tensor components and a grid search to determine location and

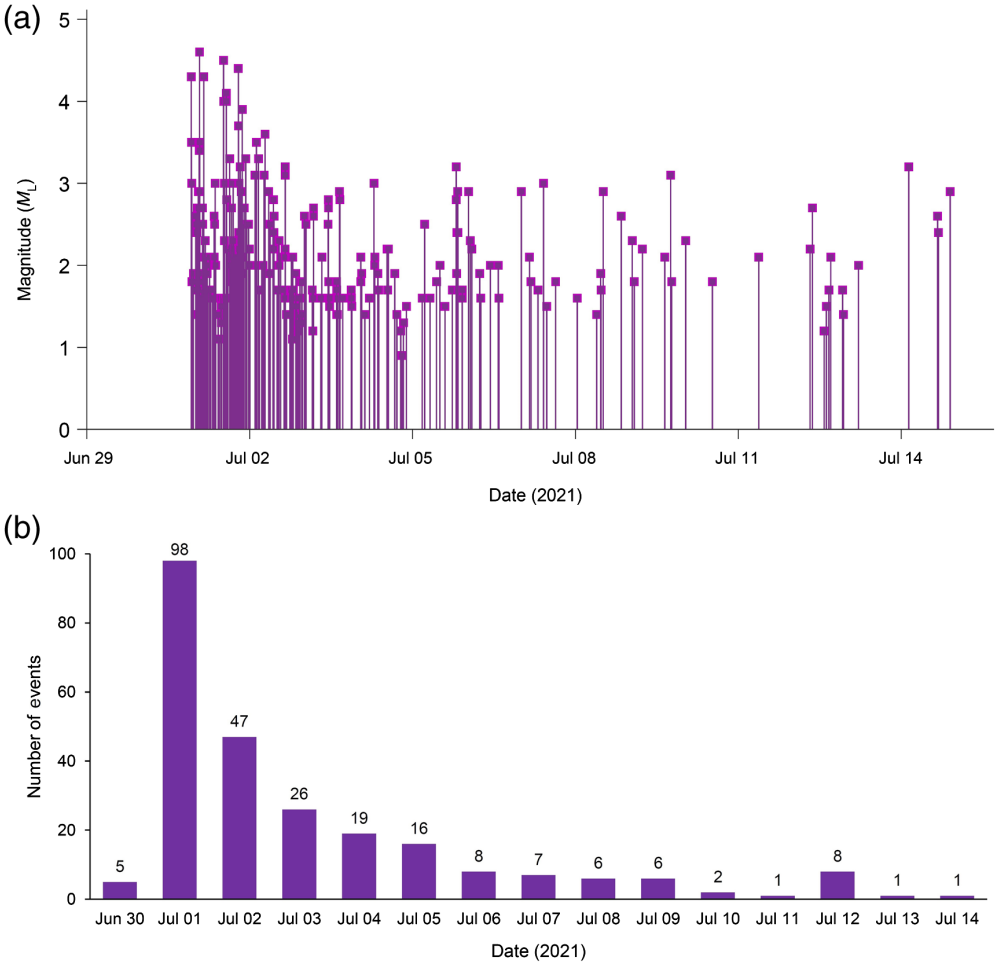

Figure 2. (a) Magnitude versus time and (b) number of events versus time for the earthquake sequence from 30 June to 14 July 2021. The color version of this figure is available only in the electronic edition.

origin time. The observed waveforms were preprocessed using a band-pass filter between 0.04 and 0.08 Hz, which was chosen based on trial and error to achieve the best waveform fitting. The data-processing stage of the source mechanism analysis is as follows: (1) convert data from Seismic Analysis Code to American Standard Code for Information Interchange format, (2) input the earthquake hypocenter locations (longitude, latitude, and depth) and origin times, (3) select stations, (4) remove the instrument response, (5) calculate the Green's function using the discrete-wavenumber method (Bouchon, 1981) to create a synthetic signal based on the velocity model, and (6) trial a specified range of source depths and origin times. For each trial, the moment tensor parameters are computed using least squares minimization based on the fit between the synthetic and observed waveform.

Results and Discussion

We relocated 254 of the 258 earthquakes that occurred in Semangko Bay using hypoDD (the remaining four were located above the surface and therefore discarded). We compare the relocated events and initial locations (as provided by the BMKG catalog) in both map and cross-section view (Fig. 3) and show that the events that had previously been held at a fixed depth are now satisfactorily relocated (Fig. 3b). The results from the bootstrap analysis method (see Data and Method section) reveal average horizontal and vertical mislocations that are typically <1 km, corresponding maximum mislocations that are <7.2 km (Fig. 4 and Fig. S3).

The focal mechanism solutions of four well-constrained events (see Figs. S4–S7 for waveform fits) consistently reveal the nodal planes to be oriented in the northwest–southeast and southwest–northeast direction (Fig. 5a). However, the horizontal distribution of seismicity does not clearly delineate a fault; therefore, it is difficult to determine which plane is the true fault plane. The A–B vertical cross section (Fig. 3), which is perpendicular to the fault plane, shows a cluster of seismicity tilted toward the southwest. This pattern corresponds to a nodal plane with a near-vertical dip and is consistent with a main fault-plane striking in a northwest–southeast direction, which corresponds to the orientation of the Sumatran fault (see Table S1). Based on the distribution of seismicity at depth (Figs. 5b and 6), we infer the graben to be in the west and the horst to be in the east, where the seismicity is on average distributed across shallower depths.

Based on the hypocenter distribution (Fig. 5b), if the fault causing these earthquakes is considered to be a single fault, it means that the fault plane is located between a depth of 2–10 km (green lines in Fig. 5b). However, the seismicity distribution extends quite far to the west (~4–5 km), which may indicate that the earthquake sequence is not caused by a single fault plane but several normal antithetic faults that are parallel to the main fault. If so, then it is likely that this region is characterized by a fairly complex graben system. The structural configuration of the area is mainly controlled by transtensional

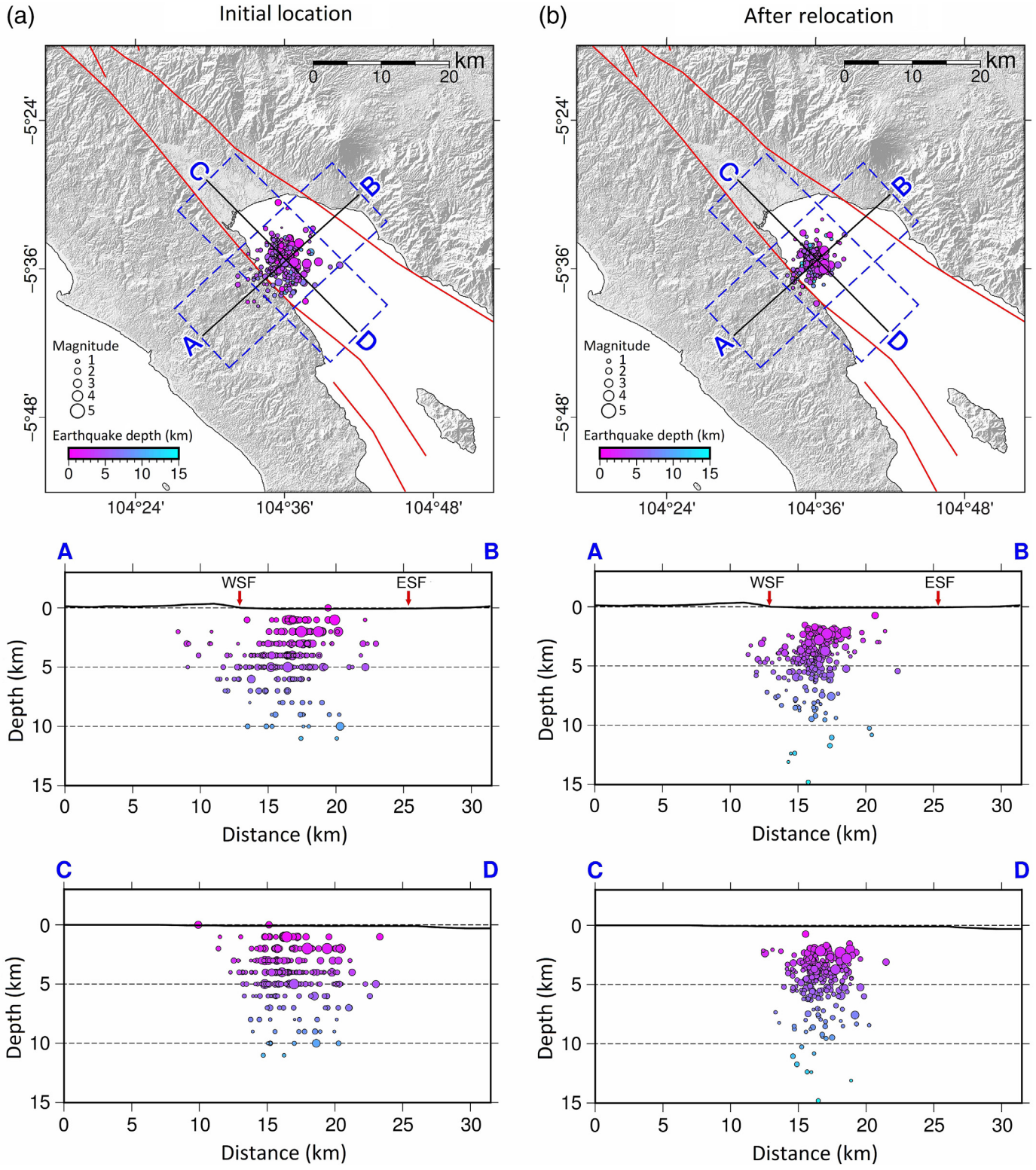

deformation along two strands of the Semangko fault that form a graben fault system. We interpret that the earthquake sequence is caused by a gradual increase in stress that affected the area, producing a high-stress concentration on multiple faults within the graben system that were subsequently activated.

Figure 3. Map view and vertical cross sections showing the earthquake sequence. (a) Initial location from the BMKG catalog and (b) after relative relocation using double-difference relocation method (hypoDD) (254 events in total). The color version of this figure is available only in the electronic edition.

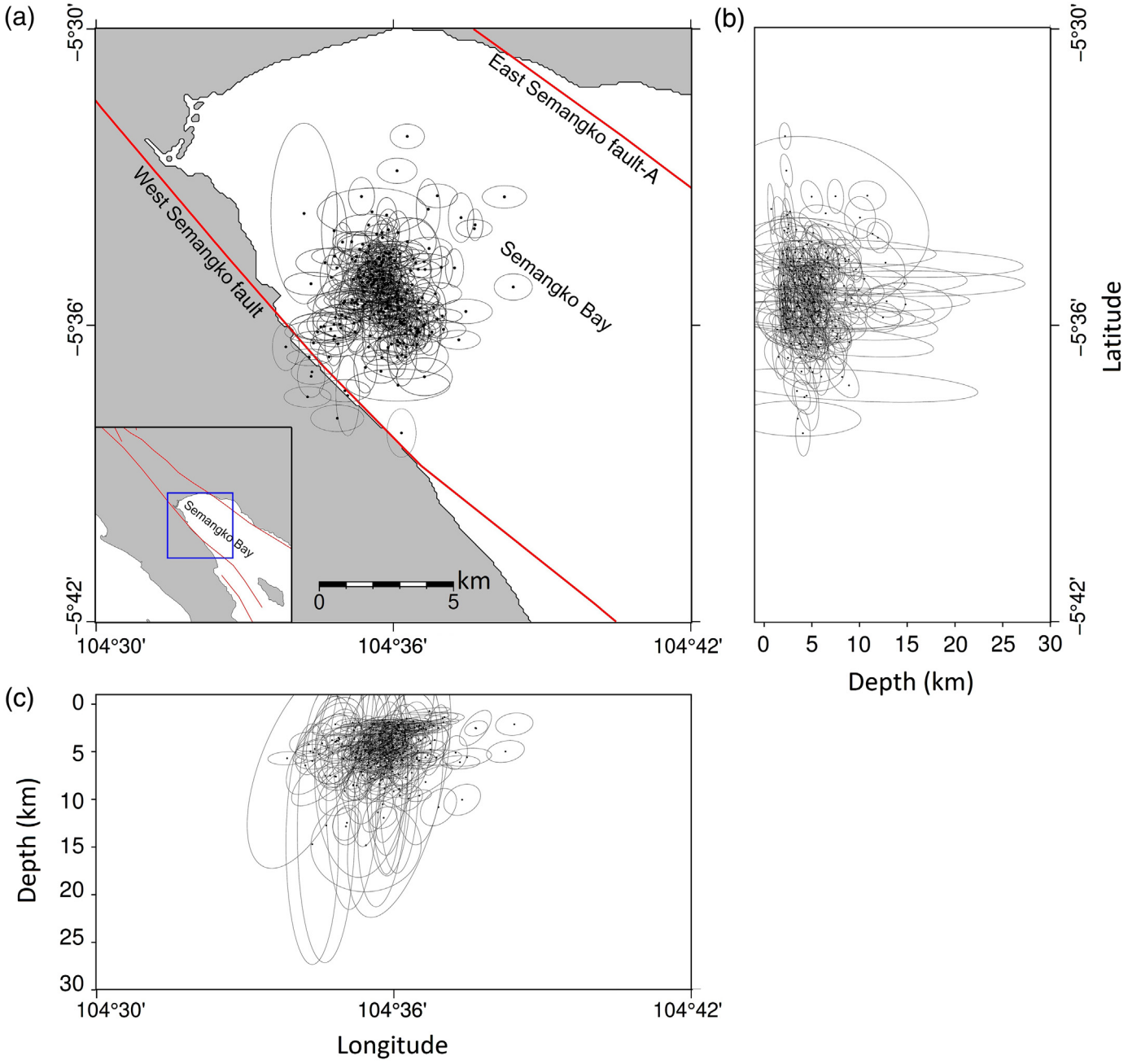

Figure 4. (a) Map view of relative location error ellipsoids at the 95% confidence level estimated for each of the earthquakes in the sequence, (b) latitude slice, and (c) longitude slice. The location of the study area is indicated in the inset. The color version of this figure is available only in the electronic edition.

Normal faults parallel to the northwest–southeast-oriented Sunda Strait graben system have been identified through analysis of multichannel seismic and bathymetric data (Susilohadi *et al.*, 2009). The graben system in the Sunda Strait is divided into two systems: the west Semangko and east Semangko grabens, which are separated by the Tabuan ridge (Susilohadi *et al.*, 2009). Based on a northeast–southwest seismic reflection profile to the south of Tabuan Island, the deepest graben is the west Semangko graben located at a depth of 2 km, with a maximum normal fault depth of 5 km. This is comparable to the depth of seismicity observed in this study, which primarily ranges between 2 and 6 km (Fig. 5b).

The Sunda Strait graben system is located between the islands of Tabuan and Panaitan. However, the presence of faults in Semangko Bay between Kota Agung and Tabuan Island has not previously been detected. The 2021 earthquake sequence points to an active graben system in the area that is bounded by the west Semangko horst to the west and Tabuan ridge to the east (Fig. 6). The eastern block, inferred to be the

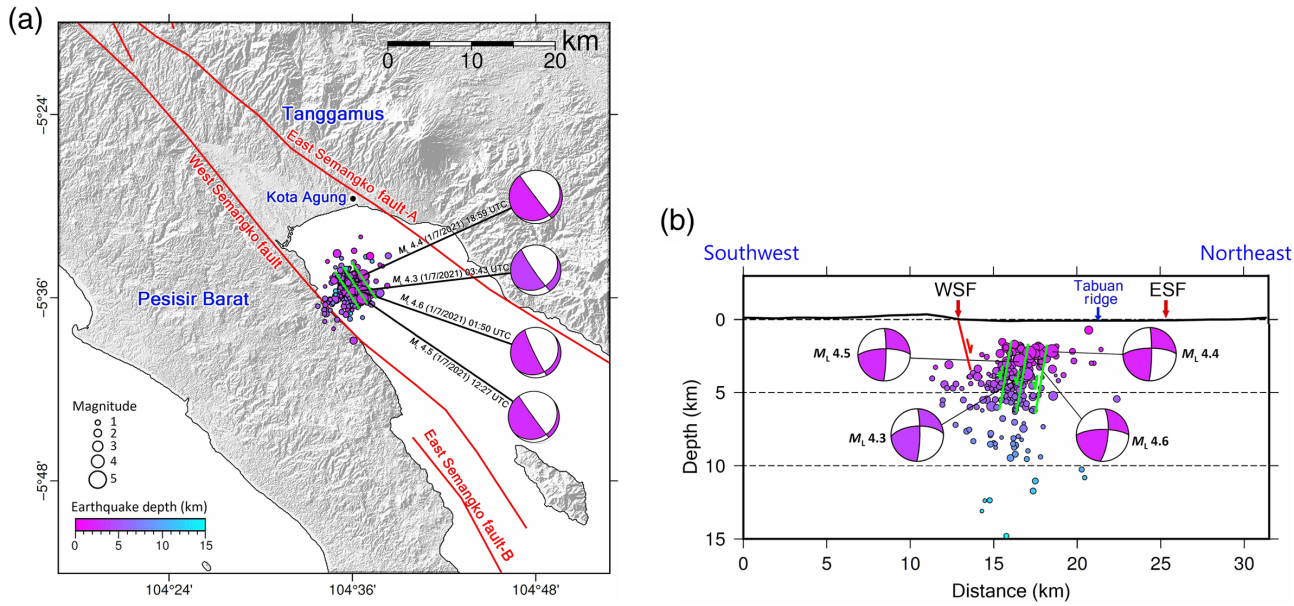

Figure 5. (a) Relocated events and focal mechanisms of a subset of the earthquake sequence in map view. Only events with a location uncertainty below 3 km are shown (233 events in total) and (b) southwest–northeast cross section illustrating how multiple faults could combine to cause the observed earthquake sequence. The solid green lines indicate the multiple faults that are antithetic to the WSF fault (red line). Focal mechanisms are plotted in a lower hemisphere projection. Each focal mechanism solution indicates a northwest–southeast-oriented fault plane that dips to the southwest at high angle. The color version of this figure is available only in the electronic edition.

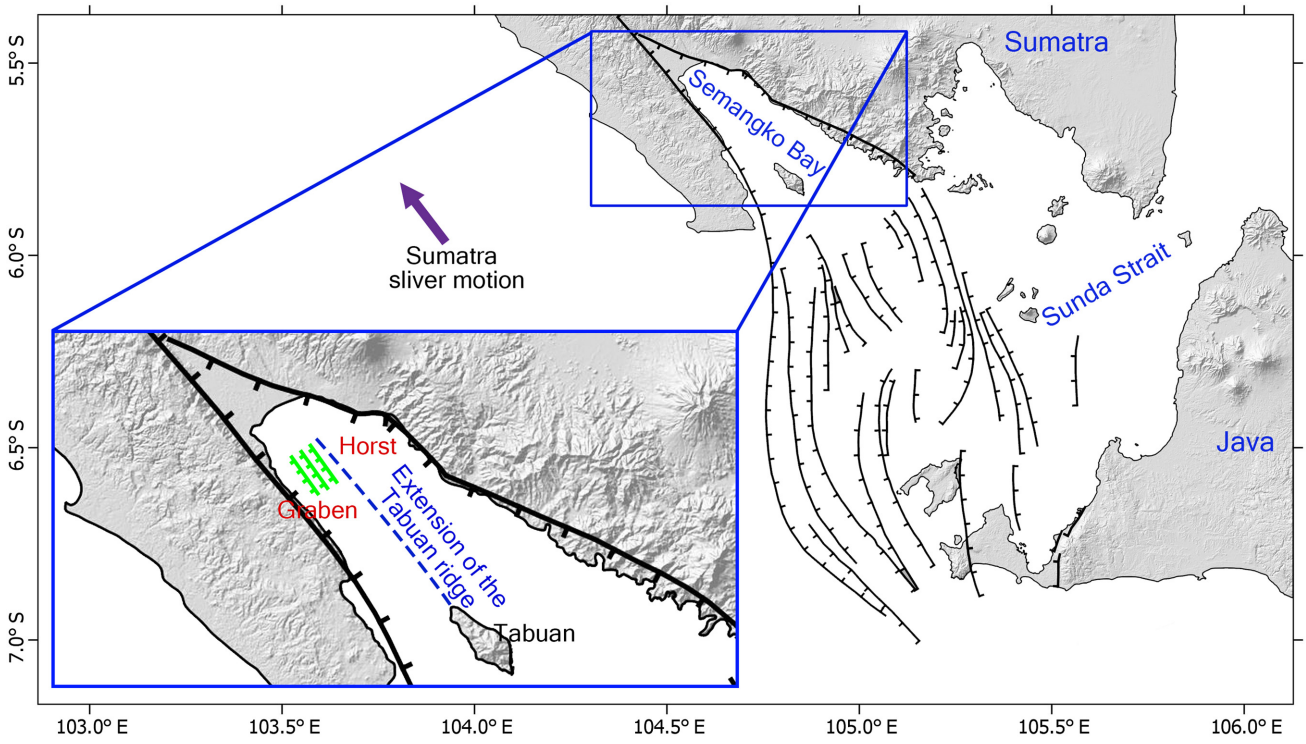

Figure 6. The interpreted location of a small graben system that may be responsible for the earthquake sequence in Semangko Bay (green lines). Major normal faults in the area have been extracted from Susilohadi *et al.* (2009), and the purple arrow depicts the direction of movement of the Sumatra sliver relative to Sundaland. The color version of this figure is available only in the electronic edition.

horst, is most likely an extension of the west Tabuan fault to the north. The existence of a graben system in Semangko Bay indicates that the area is experiencing extension in a northeast–southwest direction. This graben system, which is relatively small compared with the graben system located between Tabuan Island and Panaitan Island, indicates that the process of extension of the Sunda Strait has spread to Semangko Bay and is still ongoing today. This is supported by slip-rate estimate of the Semangko segment of the Sumatran fault, which is ~9 mm/yr (Natawidjaja, 2018).

Concluding Remarks

We have conducted hypocenter relocations and focal mechanism analysis of an atypical earthquake sequence recently detected in Semangko Bay, southern Sumatra. This sequence is front ended by a number of earthquakes in the range M_L 4.2–4.6, but no distinct mainshock is identifiable. The subsequent decay in event frequency is consistent with conventional aftershock activity. Relocated hypocenter distributions and focal mechanism solutions indicate that these events are most likely caused by the rupture of several antithetic normal faults that strike in the northwest–southeast direction, parallel to the main fault. Such an occurrence is consistent with the plate tectonic setting of the region, with clockwise rotation of Sumatra producing transtensional deformation in the Sunda Strait that manifests as active graben and horst structures across a range of scales.

Data and Resources

The earthquake dataset used in this study is sourced from Badan Meteorologi, Klimatologi, dan Geofisika (BMKG). All figures in this article and supplemental material were constructed using The Generic Mapping Tools (Wessel and Smith, 1998). Crustal faults in the region were extracted from Irsyam *et al.* (2017) and Susilohadi *et al.* (2009). Topography and bathymetry data were sourced from the Digital Elevation Model Nasional (https://tanahair.indonesia.go.id/demnas/#/demnas) and Batimetri Nasional (https://tanahair.indonesia.go.id/demnas/#/batnas). All websites were last accessed in October 2021. The earthquake relocation catalog data are available in Table S2. The supplemental material includes Figures S1–S7 and Tables S1 and S2.

Declaration of Competing Interests

The authors acknowledge that there are no conflicts of interest recorded.

Acknowledgments

Badan Meteorologi, Klimatologi, dan Geofisika (BMKG) are thanked for providing the earthquake data used in this study. The authors also acknowledge funding from Bandung Institute of Technology (ITB) through a 2021 research grant managed by ITB and awarded to S. W. This research is also funded by the University of Cambridge through a Herchel Smith Research Fellowship awarded to P. S. and was supported by Komite Kajian Gempabumi dan Tsunami BMKG.

References

Billings, S. D. (1994). Simulated annealing for earthquake location, *Geophys. J. Int.* **118,** no. 3, 680–692, doi: 10.1111/j.1365-246X.1994.tb03993.x.

Bouchon, M. (1981). A simple method to calculate Green's functions for elastic layered media, *Bull. Seismol. Soc. Am.* **71,** no. 4, 959–971, doi: 10.1785/BSSA0710040959.

Bratt, S. R., and W. Nagy (1991). *The LocSAT Program*, Science Applications International Corporation (SAIC), San Diego.

Console, R., M. Murru, P. Vannoli, R. Carluccio, M. Taroni, and G. Falcone (2020). Physics-based simulation of sequences with multiple main shocks in central Italy, *Geophys. J. Int.* **223,** no. 1, 526–542, doi: 10.1093/gji/ggaa300.

Efron, B. (1982). *The Jackknife, the Bootstrap and Other Resampling Plans*, Society for Industrial and Applied Mathematics, Philadelphia, Pennsylvania, doi: 10.1137/1.9781611970319.

Evison, F. F., and D. A. Rhoades (1993). The precursory earthquake swarm in New Zealand: Hypothesis tests, *New Zeal. J. Geol. Geophys.* **36,** no. 1, 51–60, doi: 10.1080/00288306.1993.9514553.

Hamilton, W. B. (1979). Tectonics of the Indonesian region, *Rept. 1078, Professional Paper*, doi: 10.3133/pp1078.

Hanka, W., J. Saul, B. Weber, J. Becker, P. Harjadi, F. Fauzi, and GITEWS Seismology Group (2010). Real-time earthquake monitoring for tsunami warning in the Indian Ocean and beyond, *Nat. Hazards Earth Syst. Sci.* **10,** no. 12, 2611–2622, doi: 10.5194/nhess-10-2611-2010.

Helmstetter, A., and D. Sornette (2003). Båth's law derived from the Gutenberg-Richter law and from aftershock properties, *Geophys. Res. Lett.* **30,** no. 20, doi: 10.1029/2003GL018186.

Huchon, P., and X. Le Pichon (1984). Sunda strait and central Sumatra fault, *Geol. Soc. Am.* **12,** no. 11, 668, doi: 10.1130/0091-7613(1984)12<668:SSACSF>2.0.CO;2.

Irsyam, M., S. Widiyantoro, D. H. Natawidjaja, I. Meilano, A. Rudyanto, S. Hidayati, W. Triyoso, N. R. Hanifa, D. Djarwadi, L. Faizal, *et al.* (Editors) (2017). Peta sumber dan bahaya gempa Indonesia tahun 2017, Pusat Penelitian dan Pengembangan Perumahan dan Permukiman, Badan Penelitian dan Pengembangan, Kementerian Pekerjaan Umum, Bandung, Indonesia (in Indonesian).

Kennett, B. L. N., and E. R. Engdahl (1991). Traveltimes for global earthquake location and phase identification, *Geophys. J. Int.* **105,** no. 2, 429–465, doi: 10.1111/j.1365-246X.1991.tb06724.x.

Kissling, E., W. L. Ellsworth, D. Eberhart-Phillips, and U. Kradolfer (1994). Initial reference models in local earthquake tomography, *J. Geophys. Res.* **99,** no. B10, 19635–19646, doi: 10.1029/93JB03138.

Laske, G., G. Masters, Z. Ma, and M. Pasyanos (2013). Update on CRUST1.0—A 1-degree global model of Earth's crust, *EGU General Assembly 2013, Geophysical Research Abstract*, EGU2013-2658, 2013, Vienna, Austria, 7–12 April, 2013.

Mogi, K. (1963). Some discussions on aftershocks, foreshocks and earthquake swarms: The fracture of a semi-infinite body caused by inner stress origin and its relation to the earthquake phenomena, *Bull. Earthq. Res. Inst.* **41,** 615–658.

Mukti, M. (2018). Structural style and depositional history of the Semangko pull apart basin in the southeastern segment of Sumatra fault zone, *Ris. Geo. Tam.* **28,** no. 1, 115, doi: 10.14203/risetgeotam2018.v28.954.

Natawidjaja, D. H. (2018). Updating active fault maps and sliprates along the Sumatran fault zone, Indonesia, *IOP Conf. Ser. Earth Environ. Sci.* **118,** 012001, doi: 10.1088/1755-1315/118/1/012001.

Ninkovich, D. (1976). Late cenozoic clockwise rotation of Sumatra, *Earth Planet. Sci. Lett.* **29,** no. 2, 269–275, doi: 10.1016/0012-821x(76)90130-8.

Nishimura, S., J. Nishida, T. Yokoyama, and F. Hehuwat (1986). Neo-tectonics of the Strait of Sunda, Indonesia, *J. Southeast Asian Earth Sci.* **1,** no. 2, 81–91, doi: 10.1016/0743-9547(86)90023-1.

Schlüter, H. U., C. Gaedicke, H. A. Roeser, B. Schreckenberger, H. Meyer, C. Reichert, Y. Djajadihardja, and A. Prexl (2002). Tectonic features of the southern Sumatra-western Java forearc of Indonesia: Tectonics of southern Sumatra, *Tectonics* **21,** no. 5, 11-1–11-15, doi: 10.1029/2001TC901048.

Shearer, P. M. (1997). Improving local earthquake locations using the L1 norm and waveform cross correlation: Application to the Whittier Narrows, California, aftershock sequence, *J. Geophys. Res.* **102,** no. B4, 8269–8283, doi: 10.1029/96JB03228.

Sieh, K., and D. Natawidjaja (2000). Neotectonics of the Sumatran fault, Indonesia, *J. Geophys. Res.* **105,** no. B12, 28,295–28,326, doi: 10.1029/2000JB900120.

Sokos, E. N., and J. Zahradnik (2008). ISOLA a Fortran code and a Matlab GUI to perform multiple-point source inversion of seismic data, *Comput. Geosci.* **34,** no. 8, 967–977, doi: 10.1016/j.cageo.2007.07.005.

Supendi, P., M. Ramdhan, P. Priyabudi, D. Sianipar, A. Wibowo, M. T. Gunawan, S. Rohadi, N. F. Riama, B. S. Daryono, B. S. Prayitno, *et al.* (2021). Foreshock–mainshock–aftershock sequence analysis of the 14 January 2021 (Mw 6.2) Mamuju–Majene (West Sulawesi, Indonesia) earthquake, *Earth Planets Space* **73,** no. 1, 106, doi: 10.1186/s40623-021-01436-x.

Susilohadi, S., C. Gaedicke, and Y. Djajadihardja (2009). Structures and sedimentary deposition in the Sunda Strait, Indonesia, *Tectonophysics* **467,** nos. 1/4, 55–71, doi: 10.1016/j.tecto.2008.12.015.

Waldhauser, F. (2001). hypoDD-A program to compute double-difference hypocenter locations, *Open-File Rept. 2001–113*, doi: 10.3133/ofr01113.

Waldhauser, F., and W. L. Ellsworth (2000). A double-difference earthquake location algorithm: Method and application to the northern Hayward fault, California, *Bull. Seismol. Soc. Am.* **90,** 1353–1368, doi: 10.1785/0120000006.

Wessel, P., and W. H. F. Smith (1998). New, improved version of generic mapping tools released, 47, *Eos Trans. AGU* **79,** no. 47, 579–579, doi: 10.1029/98EO00426.

Manuscript received 26 October 2021
Published online 9 February 2022